Quantification of Blood Flow in the Carotid Bifurcation of Healthy Subjects

Janna Ruisch, *Member, IEEE*, Joosje M.K. de Bakker, *Member, IEEE,* Majorie van Helvert, Erik Groot Jebbink, Suzanne Holewijn, Michel M.P.J. Reijnen, Chris L. de Korte, *Fellow, IEEE,* and Anne E.C.M. Saris, *Member, IEEE*

***Abstract*—Locally disturbed blood flow patterns are known to create an atherogenic environment, in particularly in the presence of other cardiovascular risk factors. Given the geometry of a healthy carotid artery, complex flow patterns are expected to be present. This study aims to characterize (complex) blood flow patterns and estimate flow-derived parameters in the carotid bifurcation of healthy subjects. Ultrasound-based velocity vector imaging (US-VVI) was acquired in the carotid bifurcation of twenty healthy subjects. Hemodynamic parameters, including temporal velocity profile, vector complexity, vortex presence and wall shear stress, were derived and compared between two age groups (20-30 and 65-75 years). Lower velocities and higher vector complexity values were observed in the older age group for all timepoints. The highest presence of vortices was observed during the systolic deceleration, which was more exposed in younger subjects (5 out of 10) compared to older subjects (3 out of 9). A quick build-up and consequent resolving of the vortices was reflected by the relatively short vortex duration, with a vortex presence of 11.4% (7.9-15.6) and 13.1% (5.9-18.6) as percentage of the cardiac cycle in younger and older subjects, respectively. Larger WSS estimates, represented as median along the complete vessel wall, were found in the younger subjects at all timestamps, except at systolic deceleration. In conclusion, the presence of complex flow patterns was confirmed in healthy subjects and multiple flow-derived hemodynamic parameters were evaluated in two age groups, providing an insight into age-related differences in hemodynamics. Aging seemed to result in higher vector complexities, whereas the presence of recirculating flow is less in older subjects.**

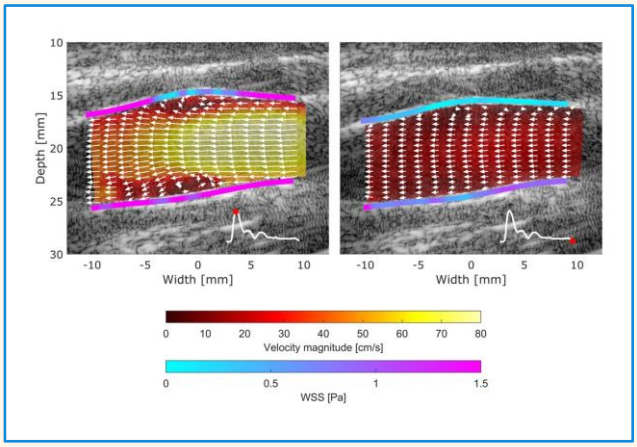

***Index Terms*—Atherosclerosis, blood flow patterns, blood speckle tracking, carotid bifurcation, hemodynamic parameters, high-frame-rate ultrasound, velocity vector imaging**

I. Introduction

Local hemodynamics play an important role in the initiation and progression of atherosclerosis [1, 2]. Complex, or disturbed flow patterns lead to regions with low and oscillating shear stress near the vessel wall, contributing to local endothelial disfunction [3]. Together with other cardiovascular risk factors, this may initiate atherosclerosis by inducing local inflammatory processes and stimuli for plaque initiation and growth [4-6]. Atherosclerosis occurs in a site-specific manner, meaning certain arterial segments, such as strong curvatures and branch points, are more susceptible to plaque development. The geometrical shape of the carotid bifurcation, including a bulbus with a larger diameter, contribute to locally disturbed blood flow and create an atherogenic environment. Given the

This paragraph of the first footnote will contain the date on which you submitted your paper for review. This work was supported in part by the Rijnstate Vriendenfonds (VF19-a10).

Janna Ruisch is with the Department of Vascular Surgery, Rijnstate Hospital, 6815 AD Arnhem, The Netherlands, and also with the Medical UltraSound Imaging Center, Department of Medical Imaging, Radboud University Medical Center, 6500 HB Nijmegen, The Netherlands (email: janna.ruisch@radboudumc.nl).

Joosje M.K. de Bakker and Anne E.C.M. Saris are with the Medical UltraSound Imaging Center, Department of Medical Imaging, Radboud University Medical Center, 6500 HB Nijmegen, The Netherlands.

Majorie van Helvert and Erik Groot Jebbink are with the Department of Vascular Surgery, Rijnstate Hospital, 6815 AD Arnhem, The Netherlands, and also with the Multi-Modality Medical Imaging group, TechMed Centre, University of Twente, 7522 NB Enschede, The Netherlands.

Suzanne Holewijn is with the Department of Vascular Surgery, Rijnstate Hospital, 6815 AD Arnhem, The Netherlands.

Michel M.P.J. Reijnen is with the Department of Vascular Surgery, Rijnstate Hospital, 6815 AD Arnhem, The Netherlands, and also with the Multi-Modality Medical Imaging group, TechMed Centre, University of Twente, 7522 NB Enschede, The Netherlands.

Chris L. de Korte is with the Medical UltraSound Imaging Center, Department of Medical Imaging, Radboud University Medical Center, 6500 HB Nijmegen, The Netherlands, and also with the Physics of Fluid group, Faculty of Science and Technology, University of Twente, 7522 NB Enschede, The Netherlands.

Highlights

- **Ultrasound-based velocity vector imaging (US-VVI) provides detailed insight in the blood flow hemodynamics of carotid bifurcations.**
- **Complex blood flow patterns are present in healthy carotid bifurcations, of which aging seems to result in the presence of more complex blood flow patterns, whereas the presence of vortices is less in older subjects.**
- **This study could serve as a first step towards a baseline reference gaining insight in age-related differences of blood flow patterns and hemodynamic parameters of carotid bifurcations.**

association between local hemodynamics and atherosclerosis, in both plaque initiation and progression, it is clinically important to localize, visualize, and quantify local blood flow patterns in the carotid bifurcation.

Conventional Duplex ultrasound is routinely applied in clinical practice to examine the condition of the carotid artery. Doppler ultrasound however, estimates the 1D velocity component along the ultrasound beam. Among others, the required manual beam-to-flow angle correction leads to large user-dependent differences in velocity values [7-9], making the technique prone to erroneous velocity measurements. Moreover, conventional Doppler ultrasound is unable to reveal the local complex blood flow dynamics in the carotid bifurcation. With the advent of ultrafast ultrasound imaging, multiple angle-independent ultrasound-based techniques have emerged that enable 2D (and even 3D) velocity vector imaging (US-VVI) in the carotid bifurcation [10-17].

Regardless of the underlying velocity estimator, these novel techniques provide 2D or 3D velocity vectors within the entire scan plane, which enables the assessment of various flow-derived parameters. Ultimately, wall shear stress (WSS), which provides direct information on the local force of blood acting on the vessel wall, can be assessed. The estimation of WSS is known to be challenging in vivo and mainly dependent on the spatiotemporal resolution of the modality to accurately obtain the velocity profiles and vessel wall contours [18]. Goudot et al. (2021) demonstrated the feasibility of WSS estimations using ultrafast velocity Doppler imaging in patients with carotid plaques and showed increased WSS at the maximum stenosis followed by low WSS downstream [19]. Furthermore, WSS values in the narrowest region of the carotid artery showed to be correlated with the degree of carotid stenosis [20]. Besides the derivation of WSS, multiple other parameters have been defined that capture flow complexity or disturbance of flow in the artery, such as vector complexity and vorticity [11, 12, 21, 22]. Vector complexity (i.e. vector concentration or Tur value, [11, 12], is a robust feature for estimating velocity angle diversity, or flow complexity in the carotid bifurcation under healthy and diseased conditions [12, 23-25]. Brandt *et al*. (2020) showed that the vector complexity during systole is strongly correlated with the carotid stenosis degree obtained by digital subtraction angiography [23]. The geometry of the carotid bulb and curvature of the carotid sinus significantly influence the local flow patterns within the vessel. Formation of vortical flow patterns, or recirculation zones, have been identified in the carotid artery, which may induce atheroprone regions [22, 26, 27]. Moreover, larger vorticity magnitudes, which indicates the curl of the velocity vector field, were observed at the base of the carotid sinus and were related with low WSS regions [28]. To summarize, previous studies suggest that these blood flow-derived metrics could provide insight into the atherosclerotic disease process by the identification of unfavorable local flow dynamics.

Given the geometry of the carotid artery, containing a bifurcation and bulb region, it is expected to find complex flow patterns in healthy vessels as well, which might initiate local atherosclerotic plaque growth in the long term. So far, novel flow-derived parameters and their effect in detecting complex blood flow patterns have been demonstrated. Still, on blood flow dynamics and the interaction of multiple flow-derived parameters in healthy carotid arteries, i.e. in the absence of atherosclerotic plaques, are lacking. Therefore, this study aims to characterize (complex) blood flow patterns and estimate flow-derived parameters in the carotid bifurcation of healthy subjects, using US-VVI. Moreover, the influence of age on blood flow patterns and blood flow metrics was investigated.

II. Method

A. Study population

This single-center, prospective, observational study included twenty healthy volunteers without cardiovascular or pulmonary history and without the use of medication for cardiovascular risk factors. The study population was equally divided into two age groups of 20-30 and 65-75 years old with an equal sex distribution. All ultrasound measurements were acquired between November 2022 and March 2023, after obtaining written informed consent. The study was approved by the institutional review board and the medical ethical committee (NL80478.091.22). The protocol was registered at *clinicalTrials.gov* (NT05451485) and the procedures were conducted conform the Declaration of Helsinki.

B. Data acquisition

Ultrasound examinations of the carotid bifurcation were performed after ten minutes in supine position, to stabilize heart rate and blood pressure. The left carotid bifurcation, including the common and internal carotid artery, was imaged in a longitudinal plane using a conventional ultrasound machine equipped with an L12-2 linear array transducer (Fujifilm Arietta 850; Fujifilm Healthcare corporation, Tokyo, Japan). Whenever anatomically possible, both the internal and external carotid artery were imaged. Conventional B-mode images and Doppler measurements were obtained at the common carotid artery, carotid bifurcation and internal carotid artery. Subsequent, the conventional ultrasound system and probe were replaced and US-VVI data were acquired at the carotid

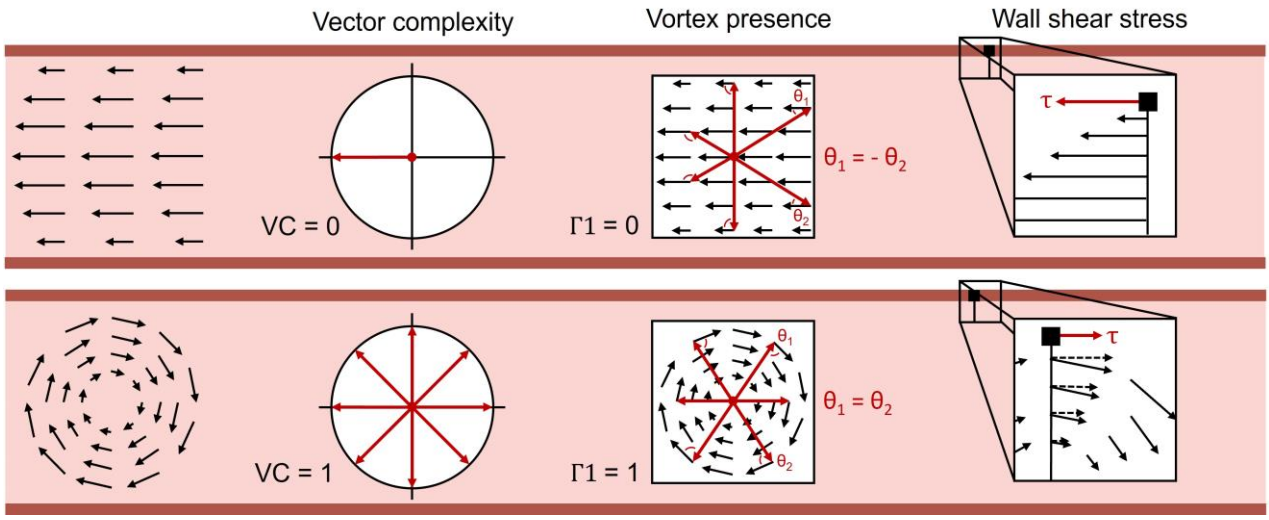

Fig. 1. A schematic representation of the flow-derived hemodynamic parameters obtained from reliable US-VVI data in the carotid bifurcation. The estimation of vector complexity (VC), vortex presence and wall shear stress (τ) are visualized for laminar (upper row) and complex flow conditions (bottom row).

bifurcation using a Verasonics Vantage 256 ultrasound system (Verasonics, Kirkland, WA, USA) equipped with an L12-5 50 mm linear array transducer (Philips (ATL), Bothwell, WA, USA). Real-time B-mode imaging was used to locate the imaging plane of interest, using the conventional images as reference. Three-seconds of raw radio-frequency (RF) channel data were acquired by transmitting plane waves at angles of -20° and 20° subsequently with a pulse repetition frequency of 10 kHz. The active transducer aperture, limited to 128 out of 256 simultaneously active elements, for the -20° and 20° steered plane waves was set such that the maximum overlap of the transmitted beams was at the depth of the carotid artery. An overview of the transducer properties and acquisition parameters is given in Table I. This imaging sequence was tested and proved to be within the thermal and mechanical safety limits for peripheral vessel applications as stated by the international standard IEC and Food and Drugs Administration [29, 30]. Intensity measurements showed a mechanical index of 0.56 and peak [negative positive] transmit pressure of [-1.97 1.72] MPa. Blood pressure and heart rate measurements were monitored (Hillrom, Welch Allyn, Skaneateles Falls, NY, USA) before and after the ultrasound examinations.

C. US-VVI

The US-VVI technique is based on blood speckle tracking, which uses pattern matching methods to estimate the displacement of speckle patterns, originating from scattering red blood cells, between two images [12]. The technique uses a plane wave ultrafast imaging sequences to minimize the time, and therefore displacement of speckle patterns generated by the fast flowing blood, between the images. The RF channel data were stored and processed offline using MATLAB (version 2021a, The MathWorks, Natick, MA, USA). RF channel data were reconstructed to RF image data, using delay-and-sum beamforming, whereafter tissue suppression was performed using an adaptive clutter filter [12]. 2D velocity vector estimates were obtained using a 2D two-iteration normalized cross-correlation based algorithm on both angles separately. The combined dual-angle compounding and single-angle projection technique, introduced by Saris et al. (2019), was used to obtain final velocity estimates, using an ensemble size of 40 frames, i.e. 39 interframe displacements, per angle. Dual-angle compounding of the angled axial estimates was performed when the normalized cross-correlation peak value was above 0.4 in >15 out of 39 interframe displacements. In case this condition was only met by one angle, projection of the single-angle estimates was performed. Estimates were defined unreliable when cross-correlation peak values were below 0.4 for both angles. Spatial median and temporal ensemble average filtering were performed to smoothen the velocity estimates. The final velocity fields obtained a sample rate of 125 velocity fields per second at a spatial resolution of 0.1 x 0.1 mm.

D. Blood flow quantification

Reliable US-VVI data in the carotid bifurcation were used to obtain multiple hemodynamic parameters: the temporal velocity profile, vector complexity, vortex presence (including size and strength), and WSS. A schematic representation of all flow-derived parameters can be seen in Fig. 1. These parameters were estimated over one complete cardiac cycle, defined as the interval between two consecutive peak systole timepoints in a dataset. Three specific timepoints during the

TABLE I
TRANSDUCER PROPERTIES AND ACQUISITION PARAMETERS

Property	Value
Center frequency (MHz)	7.8
Sampling frequency (MHz)	31.2
Transducer element pitch (μm)	195.3
Number of transducer elements	256
Number of simultaneously active elements	128
Elevational focus depth (mm)	18
Pulse repetition frequency (kHz)	10
Transmit and receive angle (°)	±20
Apodization window in transmit	Tukey (150, 30%)

cardiac cycle were studied: peak systole, systolic deceleration, and end diastole, with a fixed timestamp for the systolic deceleration at five frames, or ensembles, after peak systole. A window of five ensembles was taken around each specific timepoint and averaged to achieve a single value per timepoint.

1) Velocity

Temporal velocity profiles were obtained by spatial averaging the velocities within a trace region of 0.5 x 0.5 mm, for all velocity fields over the cardiac cycle. This trace region was manually placed in the carotid bifurcation at the location of highest velocities during peak systole. The timestamps and velocity magnitudes for the three phases in the cardiac cycle were obtained from the temporal profile.

2) Vector complexity

Vector complexity (VC), which was adapted from the vector concentration definition introduced by Pedersen *et al*. (2014), specifies the amount of spread in velocity vector directions, i.e. a measure for multi-directional flow [11, 12]. VC is defined as 1 – r, with the vector concentration (r) defined as

$$r = \frac{\sqrt{(\sum_{i=1}^{n} \cos\theta_i)^2 + (\sum_{i=1}^{n} \sin\theta_i)^2}}{n} \quad (1)$$

with θ_i the velocity vector angle of the vector at position i and n the number of vectors in the 2D velocity vector field of interest. The VC values range from 0 to 1, where 0 represents no complexity or unidirectional flow, with all velocity vectors pointing in the same direction and 1 represents the presence of fully complex flow. VC values were estimated over the full cardiac cycle, calculating a VC value for the complete carotid bifurcation within the image plane per timeframe. The time-averaged VC (VC_{TA}), i.e. the average VC over the full cardiac cycle, was derived together with VC at peak systole, systolic deceleration and end diastole.

3) Vortex presence

The locations of the center of vortices were automatically identified based on Graftieaux's method [31], using subregions S of 11 x 11 velocity vectors (1.0 x 1.0 mm^2) in the US-VVI data. Radial lines from the center of S towards the surrounding velocity vectors in S define the angle θ_n, which is the angle between the radial line and the velocity vector. The vortex identification value (Γ1) is calculated per subregion S by

$$\Gamma 1 = \frac{1}{n} \sum_S \sin(\theta_n) \quad (2)$$

with n the number of vectors in S. Γ1 values range from -1 to 1, where -1 indicates the presence of an axisymmetric counterclockwise rotation, 0 indicates laminar flow without recirculation, and +1 indicates the presence of an axisymmetric clockwise rotation. A threshold of $abs(\Gamma 1) \geq 0.70$ was used to identify a vortex, as vortices are not expected to have a perfect axisymmetric shape in vivo. To prevent false vortex detection due to spurious velocity vectors, a vortex was defined present when detected in five subsequent ensembles, i.e. 40 ms. The presence of a vortex was confirmed by visual inspection.

For each subject, the vortex duration as percentage over the full cardiac cycle (%) was defined, where 0% defines no vortex present in all frames, and 100% corresponds to the presence of one or multiple vortices in all frames of the cardiac cycle. Furthermore, in the presence of one or multiple vortices at peak systole, systolic deceleration, and/or end diastole, the maximum vortex size (mm^2) and local vorticity magnitude within the vortex region, i.e. the curl of the velocity vectors (rad/s), were estimated at these timepoints specifically. The vorticity (ω) is calculated by

$$\omega = \nabla \times \vec{v} = \frac{\partial v_y}{\partial x} - \frac{\partial v_x}{\partial y} \quad (3)$$

with ∇ the gradient operator, $\vec{v}$ the 2D velocity vector field, with horizontal and vertical velocity components (v_x, v_y) respectively. Vortex size was estimated by manually drawing an ellipse surrounding the largest vortex region, where the vortex boundaries were defined by the presence of recirculating streamlines.

4) Wall shear stress

Wall shear stress (τ) defines the amount of friction, or shear force, applied by the blood on the vessel wall and can be determined by

$$\tau = \mu \left.\frac{\partial v}{\partial r}\right|_{wall} \quad (4)$$

where μ is the blood viscosity, v is the tangential velocity with respect to the vessel wall, r the distance perpendicular to the vessel wall, and $(\partial v/\partial r)_{wall}$ is described as the shear rate measured on the vessel wall, i.e. wall shear rate (WSR).

The contours of the lumen, i.e. vessel wall position, were manually identified in the first frame of each recording and the displacement of the vessel wall was automatically estimated and accumulated over the full cardiac cycle using a 2D two-iteration normalized cross-correlation based displacement algorithm [12, 32]. Per vessel wall position, the tangential velocity vectors were calculated along a 2 mm line pointing lumen inwards, with 0.1 mm spacing. The no-slip condition was taken into account, implying that the velocity at the vessel wall surface equals zero. A second order Savitzky-Golay filter (window length 15) was used to spatially smooth the tangential velocity vectors along the 2 mm line and limit the presence of inconsistent fluctuations [18, 33]. Tangential velocities within 0.5 mm near the vessel wall were used for the WSR estimation, using the mean WSR value to estimate the WSS value at the vessel wall position. No WSR was estimated if over 50% of the velocities along the 2mm line were defined as unreliable estimates. A constant blood viscosity value of 3.5 mPa·s was used [34].

WSS was estimated for each position (distance between points ~0.8 mm) on the vessel wall and for all frames in the cardiac cycle. Per vessel wall position, the time-averaged WSS (WSS_{TA}) and oscillating shear index (WSS_{OSI}) were determined, with the prerequisite that ≥80% of WSS estimates over the cardiac cycle could be estimated. The WSS_{TA} was presented as distribution along the vessel wall using the median, minimum (1st percentile), and maximum (99th

percentile) values, providing that for ≥80% of positions on the vessel wall a reliable WSS_{TA} was estimated. WSS_{OSI} gives insight in the presence of reversing WSS directions over the cardiac cycle [1], and is determined by

$$WSS_{OSI} = \frac{1}{2}\left(1 - \frac{|\sum_1^T \tau|}{\sum_1^T |\tau|}\right) \quad (5)$$

with T the number of frames within a complete cardiac cycle, and τ as defined in (4)**.** WSS_{OSI} values range from 0, which indicates unidirectional flow, i.e. no change in WSS direction during the cardiac cycle, to 0.5 which indicates maximum possible oscillatory shear stress. The distribution of WSS_{OSI} values along the vessel wall was reported using the median and maximum (99^{th} percentile) values, again with the prerequisite that for ≥80% of the positions on the vessel wall WSS_{OSI} values are obtained.

E. Statistical analysis

Flow-derived parameters were reported per age-group (20-30 y/o and 65-75 y/o) as median and interquartile range (IQR; lower quartile – upper quartile). Age-related differences on body mass index, blood pressure, heart rate, velocities and diameters were tested using the Mann Whitney U test. Age-related difference on sex distribution was tested using the Chi-square test. Statistical analysis was performed using IMB SPSS statistics (version 27). P-values <0.05 were considered to be statistically significant.

III. Results

Baseline characteristics of all healthy subjects divided over two age groups are presented in Table II. The US-VVI recording of one carotid bulb, from the age-group of 65-75 y/o, was not successfully captured due to heavy kinking of the artery. This dataset was excluded from further analysis. Subjects in the age group of 65-75 years showed a significantly higher body mass index (p=0.001) and blood pressure (p≤0.001). Furthermore, lower peak systolic velocity (PSV) and end-diastolic velocity (EDV) values were measured in both the common and internal carotid artery in this age group.

TABLE II
BASELINE CHARACTERISTICS OF HEALTHY SUBJECTS BETWEEN TWO DIFFERENT AGE-GROUPS

	20-30 y/o (n=10)	65-75 y/o (n=9)
Age (years)	26.0 (25.3–27.5)	72.0 (69.0–73.0)
Male – n (%)	5 (50)	4 (44)
Body mass index (kg/m^2)	20.8 (20.1–23.4)	27.2 (24.5–27.8)[b]
Blood pressure (mmHg)		
Systolic	118.3 (114.0–123.6)	143.0 (138.5–155.5)[b]
Diastolic	72.3 (70.6–74.5)	84.5 (81.5–88.0)[b]
Heart rate (bpm)	61.0 (56.8–65.9)	70.5 (68.5–73.0)
Common carotid artery[a]		
PSV (cm/s)	123.0 (115.8–128.0)	93.0 (73.0–101.0)[b]
EDV (cm/s)	30.5 (27.3–35.8)	23.0 (18.0–29.0)[b]
Diameter (cm)	0.62 (0.59–0.62)	0.65 (0.60–0.71)
Internal carotid artery[a]		
PSV (cm/s)	103.0 (97.0–113.3)	85.0 (62.0–89.0)
EDV (cm/s)	35.0 (27.8–37.8)	29.0 (22.0–35.0)[b]
Diameter (cm)	0.53 (0.45–0.59)	0.50 (0.45–0.52)

Variables were expressed as median (lower quartile – upper quartile) or number (percentage). y/o = years old; PSV = peak systolic velocity; EDV = end-diastolic velocity. [a] Velocities were obtained by conventional Pulsed Wave Doppler imaging. [b] Significant difference (p<0.05) between age-groups.

Overall, good quality velocity vector estimates were obtained for all datasets. The percentage of reliable estimates, averaged over the cardiac cycle, was 97.3% (95.2–99.2) in younger subjects, compared to 82.7% (75.6–94.7) in older subjects. Small variations were observed between peak systole, systolic deceleration, and end diastole, namely 96.2% (90.0-99.3), 98.4% (95.3-99.5), and 96.9% (89.4-98.8) in younger subjects compared to 85.8% (80.1-90.9), 87.4% (82.3-94.6) and 78.4% (60.2-93.0) in older subjects, respectively.

A. Blood flow pattern in the carotid bifurcation

Three examples of US-VVI measurements are presented in Fig. 2, showing 2D blood flow patterns during systolic acceleration, peak systole, systolic deceleration, and end diastole. The corresponding movies can be found in the supplements (**Movies 1-3**). A description of the observed generic blood flow patterns in the carotid bifurcation is reported below, but specific blood flow patterns may vary between subjects. During the systolic acceleration phase, the blood pool in the full vessel is activated by the cardiac output and all velocity vectors are aligned, i.e. directed towards the internal carotid artery. Subsequent, complex blood flow patterns appeared during and directly after peak systole, where the velocity vectors point in different directions and recirculating flow regions are observed. The presence, location, and strength of these recirculating regions showed to be strongly dependent on local vessel geometry. For example, when the carotid bulb was clearly present in the image plane or when the vessel showed relatively more curvature, complex patterns were more prominent (**Movie 2)**. Complex flow patterns were absent in vessels without these geometrical features (Fig. 2, upper row and **Movie 1**). Recirculating flow patterns appeared during or after peak systole at the vascular margins of the carotid bulb region (Fig. 2, black arrows in middle row). Furthermore, the carotid flow divider also caused blood flow patterns to be complex, as the divider causes out-of-plane blood flow that shows as complex patterns in the 2D US-VVI measurements (Fig. 2, black rectangle in bottom row). This observation was clearly visible in **Movie 3**. Out-of-plane flow was observed in 11 out of 19 subjects during systole and was observed in a relative large part of the image view since the flow divider is positioned in the center of the image. Among the presence of these complex, or recirculating local regions, no general backflow was present. During the diastolic phase, complex flow patterns make room for slower forward flow, i.e. in the direction of the internal carotid, that extends towards the start of a new systolic phase.

B. Flow-derived hemodynamic parameters

The evolution of velocities, vector complexity (VC), vortex presence, and WSS over the cardiac cycle are visualized in Fig. 3 and the general hemodynamic parameters are given in Table III. Throughout the cardiac cycle, velocities were lower for the older subjects. In both age groups, the VC remained below 0.5 throughout the cardiac cycle. A small decrease in VC is observed in the systolic acceleration phase, followed by a slight increase of VC after peak systole. Overall, VC was higher in

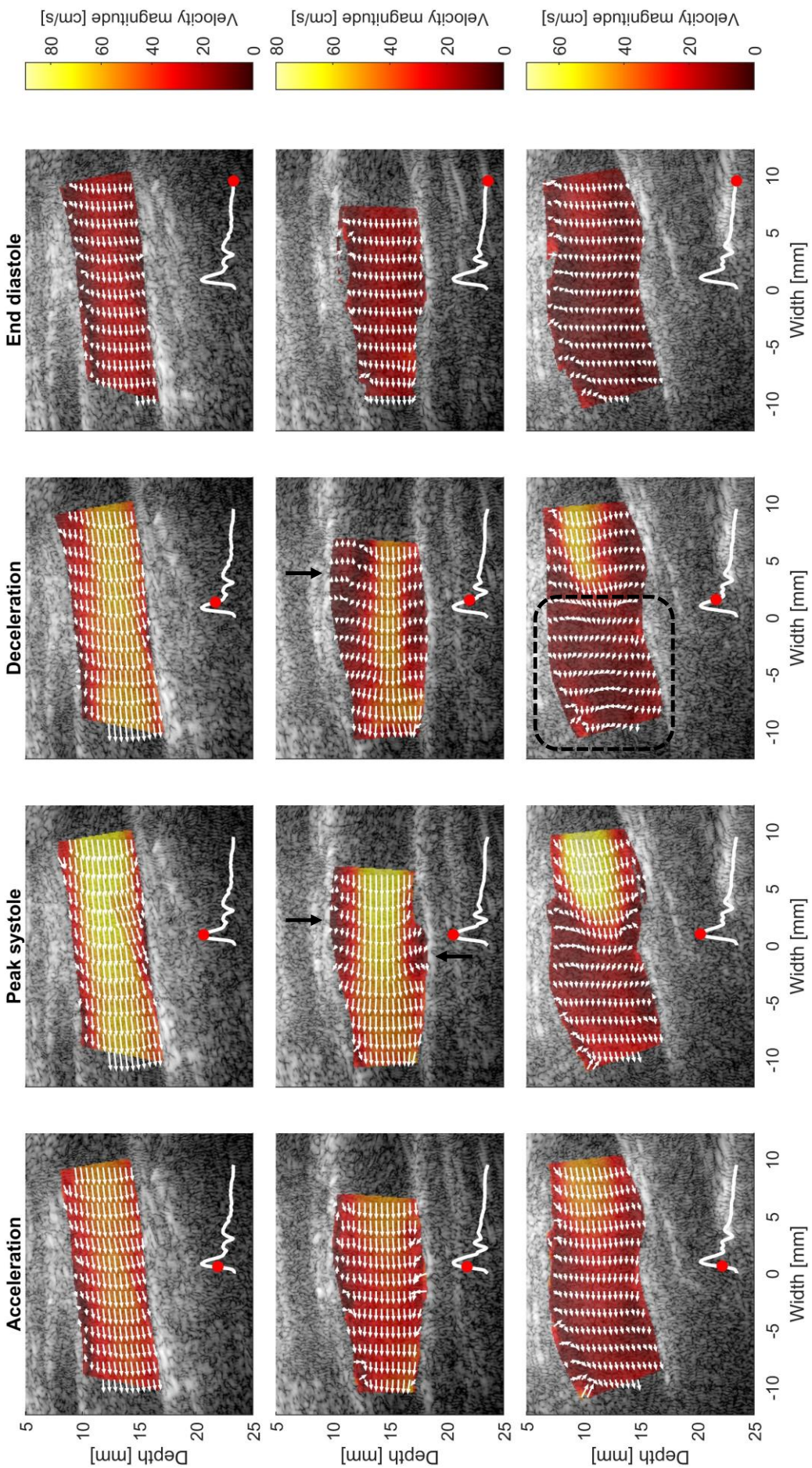

Fig. 2. Ultrasound-based velocity vector imaging in the carotid bifurcation of (upper row) a 30 y/o female, (mid row) a 24 y/o female, and (bottom row) a 67 y/o male. Velocities vectors (white) are represented on a mask of velocity magnitudes at accelerating systole, peak systole, decelerating systole and end diastole. These timepoints are annotated in the temporal profile (right-bottom corner of each image). Recirculating flow patterns were annotated with black arrows and complex blood flow patterns, caused by out-of-plane blood flow, was annotated with a black dotted rectangle.

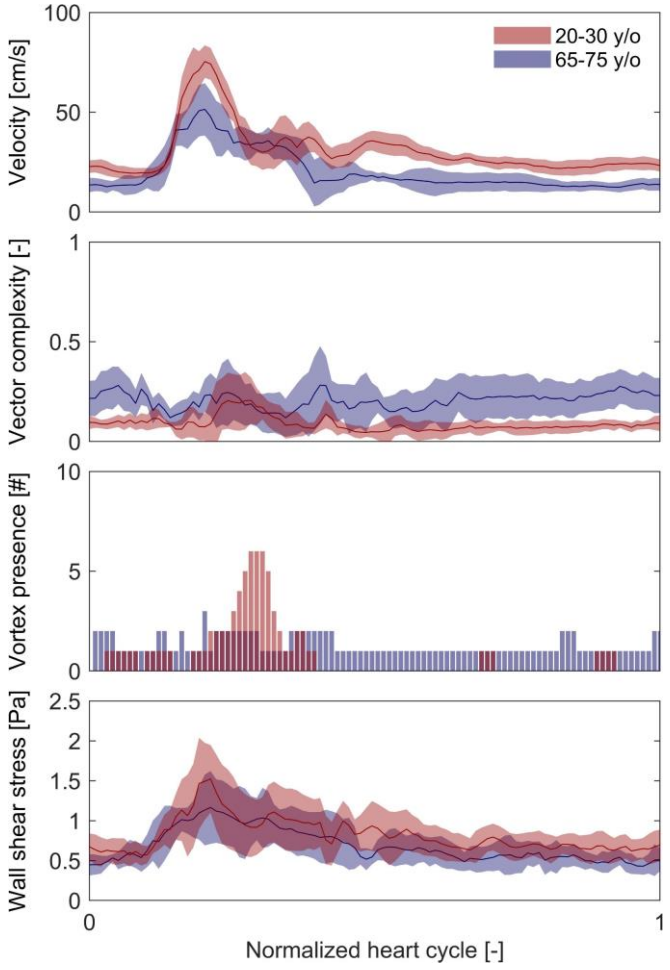

Fig. 3. The temporal velocity profiles and flow-derived parameters over a full cardiac cycle in healthy subjects of 20-30 (n=10, in red) and 65-75 years old (n=9, in blue). Velocity and vector complexity profiles are visualized as median (interquartile range). The presence of vortices (#) in each age group is shown in bars, where a vortex presence of 5 at a specific timepoint means that one or multiple vortices were found in 5 subjects of that particular age group. Note that WSS values are only shown when considered reliable (n=7 in 20-30 y/o, n=4 in 65-75 y/o).

TABLE III
FLOW FEATURES IN THE CAROTID BIFURCATION FOR TWO DIFFERENT AGE-GROUPS

	20-30 y/o (n=10)	65-75 y/o (n=9)
Time-averaged vector complexity, VC_{TA} (-)	0.08 (0.07-0.12)	0.23 (0.14-0.34)
Vortex presence (#/n)	7	5
Vortex duration (% cardiac cycle)	11.4 (7.9-15.6)	13.1 (5.9-18.6)
WSS reliable (#/n)	7 / 10	4 / 9
WSS_{TA} (Pa)		
Median	0.80 (0.60-1.12)	0.69 (0.58-0.79)
Min (1st percentile)	0.27 (0.17-0.33)	0.17 (0.14-0.21)
Max (99th percentile)	1.60 (1.18-1.87)	1.56 (1.37-1.98)
WSS_{OSI} (-)		
Median	0.00 (0.00-0.02)	0.00 (0.00-0.02)
Max (99th percentile)	0.44 (0.28-0.47)	0.49 (0.48-0.49)

Values are presented as median (lower quartile – upper quartile). y/o = years old.

the older subjects, as also represented by higher VC_{TA} values (Table III). More vortices were observed in younger subjects, with one or more vortices present in 7 out of 10 subjects, of which most vortices were identified during systolic deceleration. No difference in vortex duration was observed between the age groups, with the vortex present in 11.4% (7.9-15.6) of the cardiac cycle in younger subjects, compared to 13.1% (5.9-18.6) in the older subjects (Table III).

Reliable WSS estimates were obtained in 7 out of 10 younger subjects and 4 out of 9 older subjects. The WSS values over the cardiac cycle showed similar patterns for both age groups, with slightly higher WSS values throughout the cardiac cycle in younger subjects, which was also represented by higher WSS_{TA} values. The median WSS_{TA} distribution along the vessel wall in younger subjects was 0.80 Pa (0.60-1.12), compared to 0.69 Pa (0.58-0.79) in older subjects. No differences were observed in WSS_{OSI}, showing very low median WSS_{OSI} and high max WSS_{OSI} (Table III).

The hemodynamic parameters were also extracted specifically at peak systolic, systolic deceleration, and end-diastolic phase, see Table IV. Velocity and VC values showed similar trends as the results from Fig. 3 and Table III, with lower velocities and higher VC values in the older age group for all timepoints. At peak systole, one or more vortices are observed in two subjects in both age groups. Given the low number of identified vortices at peak systole, no conclusions can be made on vortex strength or size. More vortices were present during systolic deceleration in both age groups, whereas only one older subject showed a vortex during end diastole. Note that the vortex presence during systolic deceleration from Fig. 3 does not correspond with the numbers reported in Table IV, which can be explained by the normalization of heart cycles in Fig. 3. No substantial differences are observed in vortex size, but higher vorticity magnitudes are observed in the younger subjects during systolic deceleration. Reliable WSS estimates at these specific timepoints are obtained in 7 out of 10 younger subjects and 4 out of 9 older subjects. Larger median WSS estimates are found in the younger subjects at all timestamps, except at systolic deceleration.

In Fig. 4, a visual representation of the vortex presence and WSS estimates is shown of a 25 year old female at peak systole. The vortex location was automatically detected, of which the size was manually annotated (Fig. 4b). A relative low vector complexity (0.09) was observed in the carotid bifurcation in the presence of a small vortex (5.4 mm^2) with a low vorticity magnitude (24 rad/s). The vortex is located near the upper vessel wall, which was also represented by local low WSS estimates (Fig. 4a) and WSS_{TA} (Fig. 4c, black arrow). Low vortex duration (8.6%) was observed, with a longer duration of the vortex near the upper wall compared to the vortex near the lower wall. The upper vortex therefore causes more oscillatory behaviour of local blood flow over the cardiac cycle, resulting in local high WSS_{OSI} (Fig. 4d, black arrow).

IV. DISCUSSION

In this work, blood flow patterns were evaluated in the carotid bifurcation of healthy subjects by using the US-VVI technique. 2D blood velocity patterns were visualized and quantified in

TABLE IV
FLOW FEATURES IN THE CAROTID BIFURCATION DURING THE PEAK SYSTOLIC, SYSTOLIC DECELERATION AND END-DIASTOLIC PHASE FOR TWO DIFFERENT AGE-GROUPS

Flow features	Age group	Peak systole	Deceleration	End diastole
Velocity (cm/s)	20-30 y/o	74.3 (63.8-79.9)	59.0 (50.9-65.6)	18.9 (18.0-24.3)
	65-75 y/o	47.9 (42.3-64.1)	40.4 (32.4-54.0)	12.1 (9.7-15.4)
Vector complexity (-)	20-30 y/o	0.08 (0.06-0.15)	0.19 (0.09-0.39)	0.09 (0.05-0.12)
	65-75 y/o	0.24 (0.12-0.29)	0.23 (0.18-0.48)	0.29 (0.15-0.39)
Vortex presence (#/n)	20-30 y/o	2 / 10	5 / 10	0 / 10
	65-75 y/o	2 / 9	3 / 9	1 / 9
Vortex size (mm^2)	20-30 y/o	8.7 (7.1-10.4)	14.0 (9.6-20.6)	-
	65-75 y/o	18.4 (11.9-25.0)	10.9 (9.2-27.9)	31.4
Vorticity magnitude (rad/s)	20-30 y/o	117.5 (100.3-134.6)	94.2 (44.7-96.5)	-
	65-75 y/o	74.5 (58.8-90.3)	55.7 (42.9-65.9)	17.0
WSS reliable (#/n)	20-30 y/o	7 / 10	7 / 10	7 / 10
	65-75 y/o	4 / 9	4 / 9	4 / 9
Wall shear stress (Pa)				
Median	20-30 y/o	1.43 (0.70-1.75)	0.92 (0.69-1.36)	0.57 (0.51-0.75)
	65-75 y/o	0.97 (0.67-1.37)	1.05 (0.69-1.50)	0.43 (0.43-0.52)
Min (1^{st} percentile)	20-30 y/o	0.06 (0.03-0.12)	0.04 (0.03-0.08)	0.05 (0.04-0.06)
	65-75 y/o	0.02 (0.02-0.03)	0.04 (0.03-0.05)	0.02 (0.02-0.04)
Max (99^{th} percentile)	20-30 y/o	3.16 (2.57-3.71)	3.19 (2.45-3.40)	1.93 (1.60-2.00)
	65-75 y/o	3.01 (2.42-3.67)	2.98 (2.41-3.71)	1.27 (1.17-1.61)

Values are presented as median (lower quartile – upper quartile). y/o = years old.

high spatial and temporal resolution, allowing characterization of complex flow phenomena that vary over time and space. Different flow-derived hemodynamic parameters, such as vector complexity, vortex presence and wall shear stress, were derived from the US-VVI data, gaining insight in the hemodynamics of non-diseased carotid bifurcations.

This study confirmed the presence of complex flow patterns in healthy carotid bifurcations by using US-VVI, which was supported by the flow-derived hemodynamic parameters. Previous simulation studies reported the presence of complex, or even recirculating flow, in the carotid bifurcation of healthy subjects [26, 35]. Moreover, studies using US-VVI in the healthy carotid artery demonstrated the presence of complex flow patterns and observed vortices in the carotid sinus after peak systole [22, 25, 36], which was confirmed within the present study. Additionally, this study showed age related differences in vector complexity and the presence of vortices.

Significantly lower systolic velocities, as measured with conventional Doppler imaging, were observed in older subjects (Table II), which matches with the age trends shown in literature [37, 38]. The observed differences between younger and older subjects could be associated with age-related stiffening of the arterial system, which is also reflected by the increased blood pressures [39]. The US-VVI derived velocities confirm these findings, showing lower velocities throughout the cardiac cycle in the older subjects as well (Table IV). However, the US-VVI derived velocities are lower than the reported conventional Pulsed-Wave Doppler velocities. Besides the fact that the velocity trace position of conventional Doppler imaging did not match with US-VVI in present study, and thus these velocities should not be compared one-on-one, other studies also reported lower peak velocities in US-VVI measures compared to Pulsed-Wave Doppler [40-42], whereas good agreement was demonstrated between US-VVI and 4D flow MRI [43-45]. The velocity differences between US-VVI and Pulsed-Wave Doppler might be explained by on one side overestimation of the Pulsed-wave Doppler technique caused by intrinsic spectral broadening, overestimation due to envelope detection in the Doppler spectrum, and operator, angle, and machine dependency [44, 46, 47]. On the other hand, underestimation of the US-VVI techniques is present due to spatial and temporal smoothing [40, 44].

Overall, VC values below 0.5 were observed throughout the cardiac cycle in both age groups, which corresponds to VC values reported in earlier work [11, 12, 24, 25]. In the present study, higher VC values were found in the older group compared to the younger subjects. Dong et al. (2023) investigated the Turbulence (Tur) value, which is similar to the VC, in the CCA and carotid bulb in 40 healthy subjects within two different age groups. Dong however, observed no significant difference in Tur values between the older (50-70 years) and younger (20-49 years) subjects ($p>0.05$), but these age groups are classified differently. Differences in results might be explained by differences in sample sizes, age groups or the investigated vessel regions. This study focused on imaging the carotid bifurcation, where complex patterns are more likely to be present compared to the CCA and ICA [24]. Noticeably, the present study shows higher VC values over the complete cardiac cycle in the older group, whereas the vortex presence, i.e. the presence of recirculating flow, is less in this group. Among others, vessel geometry and age-related vessel stiffening, making it more challenging to image the vessel at the center of the lumen over the full aperture, might have caused these differences in VC [48-50]. These results show the ability of the VC parameter to estimate flow complexity, but the disability to identify local recirculating flow patterns.

Recirculating flow patterns were in general observed for a short period during systole, at the vascular margins of the carotid bulb region. To specifically detect and quantify these recirculation regions, or vortices, many research groups in the cardiac field investigated the automated localization and quantification of vortices [51-56]. However, the vortex quantification, i.e. vortex presence, size and vorticity magnitude, in carotid arteries is still limited as studies so far

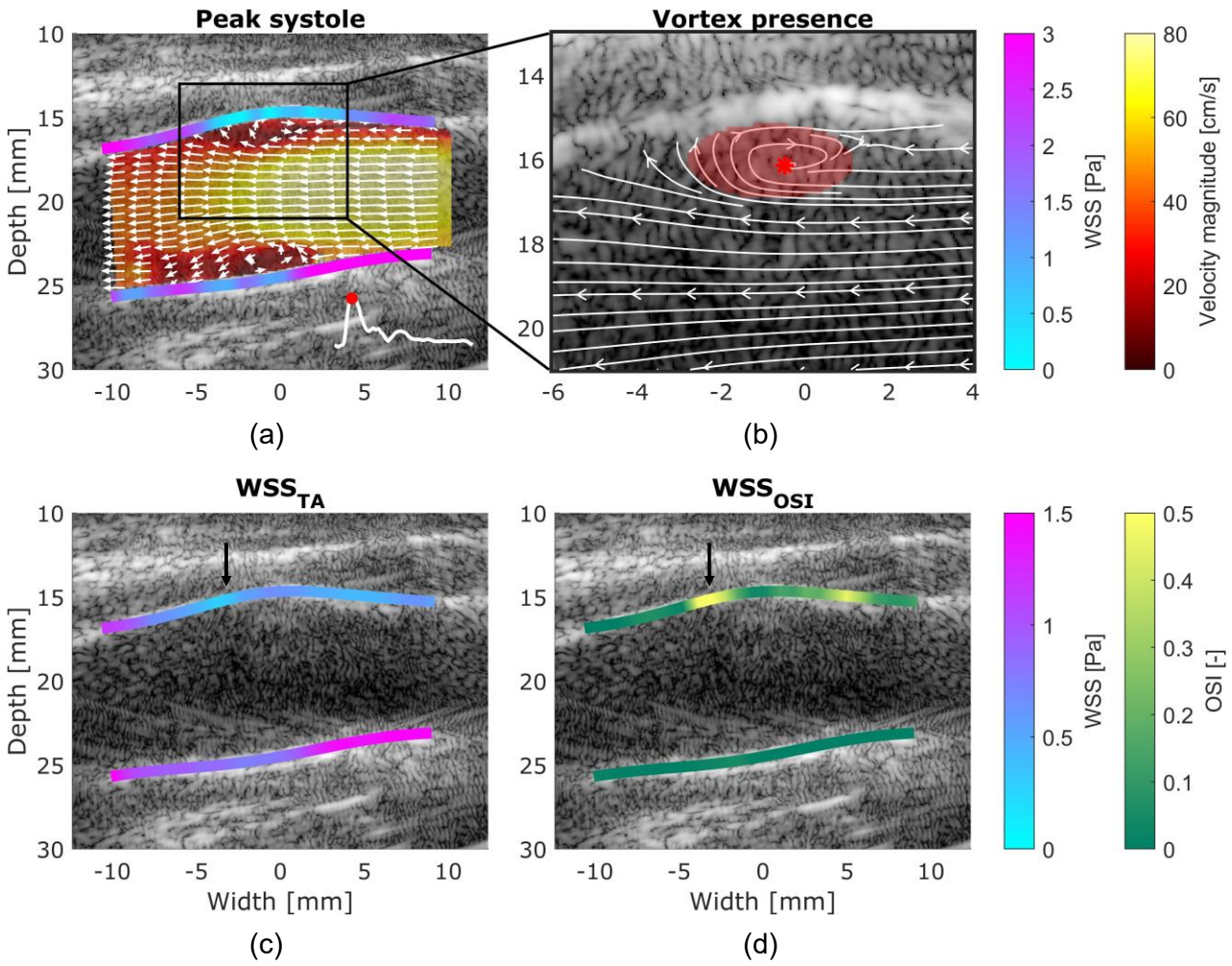

Fig. 4. (a) An example of a velocity vector field and wall shear stress (WSS) estimates of a 25 y/o female at peak systole, showing a vortex close to the upper and lower wall of the carotid bifurcation. The vector complexity of the presented frame is 0.09. The distribution of WSS along the entire vessel wall, reported as median (1^{st} – 99^{th} percentile), was 1.7 (0.07 – 3.5) Pa at peak systole, with local lower WSS at the location of the vortex. (b) A vortex was identified at the location annotated by the red star and had a size of 5.4 mm^2 (represented by red mask) and an average strength of 24 rad/s. (c-d) The distribution of time-averaged WSS (WSS_{TA}) and oscillating shear index (WSS_{OSI}) along the entire vessel wall, reported as median (1^{st} – 99^{th} percentile), was 0.8 (0.27 – 1.60) Pa and 0.02 (0.0 – 0.5), respectively. Relative low WSS_{TA} and high WSS_{OSI} were observed at the location of the vortex (black arrows).

report presence of vortices based on visual inspection of velocity fields [22, 57, 58]. In the present study, we demonstrate an automated vortex identification method for US-VVI data, using Graftieaux's method [31]. The threshold for Γ1 and minimum vortex presence of 40 ms were set to function for the carotid datasets to generate a robust vortex identification algorithm and limit erroneous vortex annotations. The detection-algorithm successfully detected both small and large vortices in our datasets, of which the presence was confirmed by visual inspection. The highest presence of vortices was observed during the systolic deceleration, which was clearly visible in subjects of 20-30 years. In this younger group, the circulatory flow regions evolve at peak systole, grow to their maximal size during the systolic deceleration and disappear at the end-systolic phase. This quick build-up and consequent resolving of the vortices is also reflected by the relatively short vortex duration over the cardiac cycle, which is in line with recent studies [22, 59]. Perrot et al. (2021) investigated the presence of backflow, which indicates among others the presence of recirculating flow, in healthy carotid arteries and observed slightly more backflow in younger subjects compared to older subjects [59]. In general, taken into account the fact that the number of vortices is limited within this dataset, all detected vortices were observed near the vessel wall, with vortex sizes ranging from 10-30 mm^2. Higher vorticity magnitudes, i.e. higher rotating motions, were observed in younger subjects, which might be due to the presence of higher velocities. The center of a vortex was automatically detected by Graftieaux's method, but the vortex size was manually delineated and defined by the presence of recirculating streamlines. In future, this should ideally be detected automatically, for example using the automated vortex identification method based on Lagrangian averaged vorticity deviation [60-62]. Moreover, clinical relevance of the

identification of vortices needs to be demonstrated and extended to diseased carotid arteries. Perrot et al. (2021) already reported substantially more backflow in diseased carotid bifurcations, which highlights the potential of this flow feature to distinguish flow in healthy and diseased carotid arteries. Besides, Wild et al. (2023) presented a correlation between vortical structures and WSS, which also highlights the essence of vortex identification in atherosclerotic diseases. The potential of vortex identification was also demonstrated in the present study in Fig. 4.

Estimating WSS using US-VVI is known to be challenging, as it requires both accurate velocity estimations near the vessel wall and correct vessel wall detection. Therefore, only a few research groups have been estimating WSS using US-VVI [19, 63-65]. With the use of a relative high center frequency resulting in high spatial resolution, adaptive high-pass finite impulse response clutter filter, and the adaptive velocity compounding method, the present study obtained WSS estimates from a velocity vector grid size of 0.1 x 0.1 mm. To ensure the trustworthiness of each WSS estimate, and the WSS-derived parameters, i.e. WSS_{TA} and WSS_{OSI}, a minimal percentage (>80%) of reliable WSS estimates was required within the full cardiac cycle and over the full vessel wall. Consequently, reliable WSS estimates were obtained in 7 out of 10 younger subjects and 4 out of 9 older subjects, demonstrating the difficulty of measuring low velocities near the vessel wall with US-VVI. Overall, lower WSS values over the full cardiac cycle were observed in the older subjects, resulting in lower WSS_{TA} values in this group. These results correspond to other work with larger sample sizes that reported a negative correlation of WSS, or WSR, but also velocity and blood volume, in the ICA and CCA with age [49, 59, 63, 65, 66]. Literature has reported on the difficulties to draw conclusions from absolute WSS values, due to the large variations between subjects [67]. In Qiu *et al.* (2020), mean WSS values of 0.75±0.25 Pa were shown at peak systole in 20-39 years old subjects and 0.49±0.11 Pa in 60-80 years old subjects [63]. These WSS values are lower compared to the median WSS at peak systole presented in Table IV. On the other hand, Samijo *et al.* (1998) observed peak WSS values of 3.59±0.8 Pa at systole in 20-29 years old subjects [66], values comparable to the max (99^{th} percentile) WSS values from Table IV. Similar values were also observed in Perrot *et al.* (2021)[59]. Although the exact measurement location is slightly different in the studies mentioned above, the comparison highlights the difficulty in evaluation of absolute WSS values and suggest that a one-on-one comparison is not feasible at the moment.

Regions with low WSS_{TA} are known to be atheroprone and are often observed in the carotid bulb in combination with high WSS_{OSI} [64, 68]. In this study, the WSS_{TA} and WSS_{OSI} results were represented as median, min (1^{st} percentile) and max (99^{th} percentile) along the complete vessel wall, but local regions of low WSS_{TA} and high WSS_{OSI} were observed in the carotid bifurcation at the location of recirculating, oscillatory flow regions (Fig. 4). Although absolute WSS values should be evaluated with care, the regions with lowest WSS are below the cutoff values for low WSS that are indicative for plaque formation as reported earlier [69, 70]. In other words, this could indicate that atheroprone regions are even observed in healthy subjects without any cardiovascular diseases.

Some limitations were present in this study. First, a small sample size was used to evaluate blood flow patterns and flow-derived hemodynamic parameters in healthy carotid bifurcations, especially for subgroups based on age that requires a correction for age-differences on BMI, blood pressure and velocities. The limited statistical power in this study restricted statistical evaluation of the presented results. Second, a selection of flow-derived hemodynamic parameters was evaluated, but there might be more potential parameters that provide insight into the hemodynamics [71]. With the current in vivo evaluation of flow-derived hemodynamic parameters in healthy carotid bifurcations, an initial basis was provided for the values of these parameters. Future research, focusing on the evaluation of blood flow patterns and flow-derived parameters in both non-diseased and diseased arteries will extend the knowledge and the prospective value of blood flow hemodynamics in the carotid bifurcation. The quality of US-VVI based on bST is known to be depth dependent [40]. Potential technical improvements, such as the use of cascaded dual-polarity wave imaging [72] or, less preferred, contrast-enhanced imaging, might improve the depth-related limitations. Parallel to this, future developments might focus on reduction of computational load to get one step closer to a real-time implementation of 2D US-VVI or even 3D imaging to capture flow in all three directions without assuming negligible out-of-plane flow [73-75].

V. Conclusion

In conclusion, US-VVI provides insight in 2D blood flow patterns in the carotid bifurcation of healthy subjects. The presence of complex flow patterns was confirmed in healthy subjects and multiple flow-derived hemodynamic parameters were evaluated in two age groups, providing an insight into age-related differences in hemodynamics. This could serve as a first step towards a baseline reference gaining insight in the hemodynamics of non-diseased carotid bifurcations. Large scale clinical studies with US-VVI in both healthy and diseased carotid arteries are needed to gain knowledge on the presence of abnormal, unfavorable blood flow patterns and improve risk stratification of patients with atherosclerotic plaques.

References

[1] D. N. Ku, D. P. Giddens, C. K. Zarins, and S. Glagov, "Pulsatile Flow and atherosclerosis in the human carotid bifurcation. Positive correlation between plaque location and low and oscillating shear stress," *Atherosclerosis*, vol. 5, 293-302, 1985, doi: 10.1161/01.atv.5.3.293.

[2] A. M. Malek, S. L. Alper, and S. Izumo, "Hemodynamic Shear Stress and its role in atherosclerosis," *JAMA*, vol. 282, pp. 2035-2042, 1999, doi: 10.1001/jama.282.21.2035.

[3] J. Zhou, Y. S. Li, and S. Chien, "Shear stress-initiated signaling and its regulation of endothelial function,"

Arterioscler Thromb Vasc Biol, vol. 34, no. 10, pp. 2191-8, Oct 2014, doi: 10.1161/ATVBAHA.114.303422.

[4] M. Cibis *et al.*, "Relation between wall shear stress and carotid artery wall thickening MRI versus CFD," *J Biomech*, vol. 49, no. 5, pp. 735-741, Mar 21 2016, doi: 10.1016/j.jbiomech.2016.02.004.

[5] C. Carallo, C. Tripolino, M. S. De Franceschi, C. Irace, X. Y. Xu, and A. Gnasso, "Carotid endothelial shear stress reduction with aging is associated with plaque development in twelve years," *Atherosclerosis*, vol. 251, pp. 63-69, Aug 2016, doi: 10.1016/j.atherosclerosis.2016.05.048.

[6] C. Strecker *et al.*, "Carotid Geometry and Wall Shear Stress Independently Predict Increased Wall Thickness-A Longitudinal 3D MRI Study in High-Risk Patients," *Front Cardiovasc Med*, vol. 8, p. 723860, 2021, doi: 10.3389/fcvm.2021.723860.

[7] P. Tortoli, M. Lenge, D. Righi, G. Ciuti, H. Liebgott, and S. Ricci, "Comparison of carotid artery blood velocity measurements by vector and standard Doppler approaches," *Ultrasound Med Biol*, vol. 41, no. 5, pp. 1354-62, May 2015, doi: 10.1016/j.ultrasmedbio.2015.01.008.

[8] B. M. Eicke, F. W. Kremkau, H. Hinson, and C. H. Tegeler, "Peak Velocity Overestimation and Linear array spectral Doppler," *J Neuroimag*, vol. 5, pp. 115-121, 1995, doi: 10.1111/jon199552115.

[9] T. Jogestrand, M. Lindqvist, and J. Nowak, "Diagnostic Performance of Duplex Ultrasonography in the Detection of High Grade Internal Carotid Artery Stenosis," *Eur J Vasc Endovasc Surg*, vol. 23, pp. 510-518, 2002, doi: 10.1053/ejvs.2002.1621.

[10] J. Jensen *et al.*, "Accuracy and Precision of a Plane Wave Vector Flow Imaging Method in the Healthy Carotid Artery," *Ultrasound Med Biol*, vol. 44, no. 8, pp. 1727-1741, Aug 2018, doi: 10.1016/j.ultrasmedbio.2018.03.017.

[11] M. M. Pedersen *et al.*, "Novel flow quantification of the carotid bulb and the common carotid artery with vector flow ultrasound," *Ultrasound Med Biol*, vol. 40, no. 11, pp. 2700-6, Nov 2014, doi: 10.1016/j.ultrasmedbio.2014.06.001.

[12] A. Saris, H. H. G. Hansen, S. Fekkes, J. Menssen, M. M. Nillesen, and C. L. de Korte, "In Vivo Blood Velocity Vector Imaging Using Adaptive Velocity Compounding in the Carotid Artery Bifurcation," *Ultrasound Med Biol*, vol. 45, no. 7, pp. 1691-1707, Jul 2019, doi: 10.1016/j.ultrasmedbio.2019.03.008.

[13] M. Correia, J. Provost, M. Tanter, and M. Pernot, "4D ultrafast ultrasound flow imaging: in vivo quantification of arterial volumetric flow rate in a single heartbeat," *Phys Med Biol*, vol. 61, no. 23, pp. L48-L61, Dec 7 2016, doi: 10.1088/0031-9155/61/23/L48.

[14] A. H. Brandt *et al.*, "A Comparison Study of Vector Velocity, Spectral Doppler and Magnetic Resonance of Blood Flow in the Common Carotid Artery," *Ultrasound Med Biol*, vol. 44, no. 8, pp. 1751-1761, Aug 2018, doi: 10.1016/j.ultrasmedbio.2018.05.002.

[15] S. Fadnes, I. K. Ekroll, S. A. Nyrnes, H. Torp, and L. Lovstakken, "Robust angle-independent blood velocity estimation based on dual-angle plane wave imaging," *IEEE Trans Ultrason Ferroelectr Freq Control*, vol. 62, no. 10, pp. 1757-67, Oct 2015, doi: 10.1109/TUFFC.2015.007108.

[16] K. L. Hansen, J. Udesen, F. Gran, J. A. Jensen, and M. Bachmann Nielsen, "In-vivo examples of flow patterns with the fast vector velocity ultrasound method," *Ultraschall Med*, vol. 30, pp. 471-477, 2009, doi: 10.1055/s-0028-1109572.

[17] C. A. Villagomez Hoyos, M. B. Stuart, K. L. Hansen, M. B. Nielsen, and J. A. Jensen, "Accurate Angle Estimator for High-Frame-Rate 2-D Vector Flow Imaging," *IEEE Trans Ultrason Ferroelectr Freq Control*, vol. 63, no. 6, pp. 842-53, Jun 2016, doi: 10.1109/TUFFC.2016.2551689.

[18] C. H. Leow and M. X. Tang, "Spatio-Temporal Flow and Wall Shear Stress Mapping Based on Incoherent Ensemble-Correlation of Ultrafast Contrast Enhanced Ultrasound Images," *Ultrasound Med Biol*, vol. 44, no. 1, pp. 134-152, Jan 2018, doi: 10.1016/j.ultrasmedbio.2017.08.930.

[19] G. Goudot *et al.*, "Wall Shear Stress Measurement by Ultrafast Vector Flow Imaging for Atherosclerotic Carotid Stenosis," *Ultraschall Med*, vol. 42, no. 3, pp. 297-305, Jun 2021, doi: 10.1055/a-1060-0529.

[20] Y. Qiu *et al.*, "High-Frame Rate Vector Flow Imaging Technique: Initial Application in Evaluating the Hemodynamic Changes of Carotid Stenosis Caused by Atherosclerosis," *Front Cardiovasc Med*, vol. 8, p. 617391, 2021, doi: 10.3389/fcvm.2021.617391.

[21] K. L. Hansen, "Vector concentration - a new ultrasound parameter for stenosis assessment using vector flow imaging," *Cardiovascular Imaging*, pp. 19-21, 2019.

[22] A. Goddi *et al.*, "High-Frame Rate Vector Flow Imaging of the Carotid Bifurcation in Healthy Adults: Comparison With Color Doppler Imaging," *J Ultrasound Med*, vol. 37, no. 9, pp. 2263-2275, Sep 2018, doi: 10.1002/jum.14579.

[23] A. H. Brandt *et al.*, "Carotid Stenosis Assessment with Vector Concentration before and after Stenting," *Diagnostics (Basel)*, vol. 10, no. 6, Jun 20 2020, doi: 10.3390/diagnostics10060420.

[24] Y. Dong *et al.*, "Blood Flow Turbulence Quantification of Carotid Artery With a High-Frame Rate Vector Flow Imaging," *J Ultrasound Med*, vol. 42, no. 2, pp. 427-436, Feb 2023, doi: 10.1002/jum.16039.

[25] S. Hong *et al.*, "Precise evaluation of blood flow patterns in human carotid bifurcation based on high-frame-rate vector flow imaging," *J Clin Ultrasound*, vol. 51, no. 6, pp. 1070-1077, Jul-Aug 2023, doi: 10.1002/jcu.23489.

[26] Y. Chen, X. Yang, A. J. Iskander, and P. Wang, "On the flow characteristics in different carotid arteries,"

Physics of Fluids, vol. 32, no. 10, 2020, doi: 10.1063/5.0022092.

[27] C. C. M. Rindt and A. A. Steenhoven, "Unsteady Flow in a Rigid 3D Model of the Carotid Artery Bifurcation," *Biomedical Engineering*, vol. 118, pp. 90-96, 1996, doi: 10.1115/1.2795950.

[28] N. Kumar, R. Pai, M. S. Manjunath, A. Ganesha, and S. M. Abdul Khader, "Effect of linear and Mooney–Rivlin material model on carotid artery hemodynamics," *Journal of the Brazilian Society of Mechanical Sciences and Engineering*, vol. 43, no. 8, 2021, doi: 10.1007/s40430-021-03110-5.

[29] "Medical electrical equipment - Part 2-37: Particular requiments for the safety of ultrasonic medical diagnostic and monitoring equipment.," 2015. [Online]. Available: https://webstore.iec.ch/publication/22634.

[30] FDA, "Marketing Clearance of Diagnostic Ultrasound Systems and Transducers," *Food Drug Admin.*, 2024. [Online]. Available: https://www.fda.gov/regulatory-information/search-fda-guidance-/marketing-clearance-diagnostic-ultrasound-systems-and-transducers.

[31] L. Graftieaux, M. Michard, and N. Grosjean, "Combining PIV, POD and vortex identification algorithms for the study of unsteady turbulent swirling flows," *Meas. Sci. Technol.*, vol. 12, pp. 1422-1429, 2001, doi: 10.1088/0957-0233/12/9/307.

[32] R. G. Lopata, M. M. Nillesen, H. H. Hansen, I. H. Gerrits, J. M. Thijssen, and C. L. de Korte, "Performance evaluation of methods for two-dimensional displacement and strain estimation using ultrasound radio frequency data," *Ultrasound Med Biol*, vol. 35, no. 5, pp. 796-812, May 2009, doi: 10.1016/j.ultrasmedbio.2008.11.002.

[33] K. Yang, P. R. Hoskins, G. A. Corner, C. Xia, and Z. Huang, "Wall Shear Stress Measurement in Carotid Artery Phantoms with Variation in Degree of Stenosis Using Plane Wave Vector Doppler," *Applied Sciences*, vol. 13, no. 1, 2023, doi: 10.3390/app13010617.

[34] Y. Du *et al.*, "Wall Shear Stress Measurements Based on Ultrasound Vector Flow Imaging: Theoretical Studies and Clinical Examples," *J Ultrasound Med*, vol. 39, no. 8, pp. 1649-1664, Aug 2020, doi: 10.1002/jum.15253.

[35] I. Marshall, P. Papathanasopoulou, and K. Wartolowska, "Carotid flow rates and flow division at the bifurcation in healthy volunteers," *Physiol Meas*, vol. 25, no. 3, pp. 691-7, Jun 2004, doi: 10.1088/0967-3334/25/3/009.

[36] J. Udesen, M. B. Nielsen, K. R. Nielsen, and J. A. Jensen, "Examples of in vivo blood vector velocity estimation," *Ultrasound Med Biol*, vol. 33, no. 4, pp. 541-8, Apr 2007, doi: 10.1016/j.ultrasmedbio.2006.10.014.

[37] J. M. Kotchen, M. P. H. Harlley, H. E. McKean, and T. A. Kotchen, "Blood pressure trends with aging," *Hypertension*, III, pp. 128-134, 1982, doi: 10.1161/01.hyp.4.5_pt_2.iii128.

[38] K. Hirata, T. Yaginuma, M. F. O'Rourke, and M. Kawakami, "Age-related changes in carotid artery flow and pressure pulses: possible implications for cerebral microvascular disease," *Stroke*, vol. 37, no. 10, pp. 2552-6, Oct 2006, doi: 10.1161/01.STR.0000242289.20381.f4.

[39] J. C. Kohn, M. C. Lampi, and C. A. Reinhart-King, "Age-related vascular stiffening: causes and consequences," *Front Genet*, vol. 6, p. 112, 2015, doi: 10.3389/fgene.2015.00112.

[40] S. A. Nyrnes, S. Fadnes, M. S. Wigen, L. Mertens, and L. Lovstakken, "Blood Speckle-Tracking Based on High-Frame Rate Ultrasound Imaging in Pediatric Cardiology," *J Am Soc Echocardiogr*, vol. 33, no. 4, pp. 493-503 e5, Apr 2020, doi: 10.1016/j.echo.2019.11.003.

[41] I. K. Ekroll, A. Swillens, P. Segers, T. Dahl, H. Torp, and L. Lovstakken, "Simultaneous quantification of flow and tissue velocities based on multi-angle plane wave imaging," *IEEE Trans Ultrason Ferroelectr Freq Control*, vol. 60, no. 4, pp. 727-38, Apr 2013, doi: 10.1109/TUFFC.2013.2621.

[42] M. Strachinaru *et al.*, "Left ventricular high frame rate echo-particle image velocimetry: clinical application and comparison with conventional imaging," *Cardiovasc Ultrasound*, vol. 20, no. 1, p. 11, Apr 26 2022, doi: 10.1186/s12947-022-00283-4.

[43] Y. Han *et al.*, "Validation of Left Ventricular High Frame Rate Echo-Particle Image Velocimetry against 4D Flow MRI in Patients," 2024, doi: 10.1101/2023.11.27.23298719.

[44] Y. Du *et al.*, "Quantitative Blood Flow Measurements in the Common Carotid Artery: A Comparative Study of High-Frame-Rate Ultrasound Vector Flow Imaging, Pulsed Wave Doppler, and Phase Contrast Magnetic Resonance Imaging," *Diagnostics (Basel)*, vol. 12, no. 3, Mar 11 2022, doi: 10.3390/diagnostics12030690.

[45] M. van Helvert *et al.*, "High-Frame-Rate Ultrasound Velocimetry in the Healthy Femoral Bifurcation: A Comparative Study Against 4-D Flow Magnetic Resonance Imaging," *Ultrasound Med Biol*, Sep 6 2024, doi: 10.1016/j.ultrasmedbio.2024.05.013.

[46] S. Ambrogio *et al.*, "Pulsed Wave Doppler Measurements of Maximum Velocity: Dependence on Sample Volume Size," *Ultrasound Med Biol*, vol. 48, no. 1, pp. 68-77, Jan 2022, doi: 10.1016/j.ultrasmedbio.2021.09.006.

[47] G. Guidi, C. Licciardello, and S. Falteri, "Intrinsic spectral broadening (ISB) in ultrasound Doppler as combination of transit time and local geometrical broadening," *Ultrasound Med Biol*, vol. 26, no. 5, pp. 853-862, 2000, doi: 10.1016/s0301-5629(00)00218-0.

[48] T. Saho and H. Onishi, "Evaluation of the impact of carotid artery bifurcation angle on hemodynamics by use of computational fluid dynamics: a simulation and volunteer study," *Radiol Phys Technol*, vol. 9, no. 2,

pp. 277-85, Jul 2016, doi: 10.1007/s12194-016-0360-7.

[49] G. Zhang *et al.*, "Age and anatomical location related hemodynamic changes assessed by 4D flow MRI in the carotid arteries of healthy adults," *Eur J Radiol*, vol. 128, p. 109035, Jul 2020, doi: 10.1016/j.ejrad.2020.109035.

[50] A. V. Kamenskiy, Pipinos, II, J. S. Carson, J. N. MacTaggart, and B. T. Baxter, "Age and disease-related geometric and structural remodeling of the carotid artery," *J Vasc Surg*, vol. 62, no. 6, pp. 1521-8, Dec 2015, doi: 10.1016/j.jvs.2014.10.041.

[51] G. R. Hong *et al.*, "Characterization and quantification of vortex flow in the human left ventricle by contrast echocardiography using vector particle image velocimetry," *JACC Cardiovasc Imaging*, vol. 1, no. 6, pp. 705-17, Nov 2008, doi: 10.1016/j.jcmg.2008.06.008.

[52] K. H. Park *et al.*, "Characterization of the left atrial vortex flow by two-dimensional transesophageal contrast echocardiography using particle image velocimetry," *Ultrasound Med Biol*, vol. 39, no. 1, pp. 62-71, Jan 2013, doi: 10.1016/j.ultrasmedbio.2012.08.013.

[53] G. Pedrizzetti, G. La Canna, O. Alfieri, and G. Tonti, "The vortex--an early predictor of cardiovascular outcome?," *Nat Rev Cardiol*, vol. 11, no. 9, pp. 545-53, Sep 2014, doi: 10.1038/nrcardio.2014.75.

[54] D. Mele *et al.*, "Intracardiac Flow Analysis: Techniques and Potential Clinical Applications," *J Am Soc Echocardiogr*, vol. 32, no. 3, pp. 319-332, Mar 2019, doi: 10.1016/j.echo.2018.10.018.

[55] A. Fiorencis *et al.*, "Noninvasive Evaluation of Intraventricular Flow Dynamics by the HyperDoppler Technique: First Application to Normal Subjects, Athletes, and Patients with Heart Failure," *J Clin Med*, vol. 11, no. 8, Apr 15 2022, doi: 10.3390/jcm11082216.

[56] F. Mehregan *et al.*, "Doppler vortography: a color Doppler approach to quantification of intraventricular blood flow vortices," *Ultrasound Med Biol*, vol. 40, no. 1, pp. 210-21, Jan 2014, doi: 10.1016/j.ultrasmedbio.2013.09.013.

[57] N. C. Wild, K. V. Bulusu, and M. W. Plesniak, "Vortical Structures Promote Atheroprotective Wall Shear Stress Distributions in a Carotid Artery Bifurcation Model," *Bioengineering (Basel)*, vol. 10, no. 9, Sep 3 2023, doi: 10.3390/bioengineering10091036.

[58] H. Jung *et al.*, "Comparison of haemodynamics in carotid endarterectomy: primary closure versus patch angioplasty," *Engineering Applications of Computational Fluid Mechanics*, vol. 16, no. 1, pp. 1601-1618, 2022, doi: 10.1080/19942060.2022.2102078.

[59] V. Perrot *et al.*, "Translation of Simultaneous Vessel Wall Motion and Vectorial Blood Flow Imaging in Healthy and Diseased Carotids to the Clinic: A Pilot Study," *IEEE Trans Ultrason Ferroelectr Freq Control*, vol. 68, no. 3, pp. 558-569, Mar 2021, doi: 10.1109/TUFFC.2020.3015340.

[60] K. Yang, S. Wu, D. N. Ghista, D. Yang, and K. K. L. Wong, "Automated vortex identification based on Lagrangian averaged vorticity deviation in analysis of blood flow in the atrium from phase contrast MRI," *Comput Methods Programs Biomed*, vol. 216, p. 106678, Apr 2022, doi: 10.1016/j.cmpb.2022.106678.

[61] K. Yang *et al.*, "A Hybrid Approach for Cardiac Blood Flow Vortex Ring Identification Based on Optical Flow and Lagrangian Averaged Vorticity Deviation," *Front Physiol*, vol. 12, p. 698405, 2021, doi: 10.3389/fphys.2021.698405.

[62] G. Haller, A. Hadjighasem, M. Farazmand, and F. Huhn, "Defining coherent vortices objectively from the vorticity," *Journal of Fluid Mechanics*, vol. 795, pp. 136-173, 2016, doi: 10.1017/jfm.2016.151.

[63] Y. Qiu, D. Yang, Q. Zhang, K. Chen, Y. Dong, and W. P. Wang, "V Flow technology in measurement of wall shear stress of common carotid arteries in healthy adults: Feasibility and normal values," *Clin Hemorheol Microcirc*, vol. 74, no. 4, pp. 453-462, 2020, doi: 10.3233/CH-190719.

[64] A. J. Y. Chee, C. K. Ho, B. Y. S. Yiu, and A. C. H. Yu, "Time-Resolved Wall Shear Rate Mapping Using High-Frame-Rate Ultrasound Imaging," *IEEE Trans Ultrason Ferroelectr Freq Control*, vol. 69, no. 12, pp. 3367-3381, Dec 2022, doi: 10.1109/TUFFC.2022.3220560.

[65] K. Saito *et al.*, "Blood Flow Visualization and Wall Shear Stress Measurement of Carotid Arteries Using Vascular Vector Flow Mapping," *Ultrasound Med Biol*, vol. 46, no. 10, pp. 2692-2699, Oct 2020, doi: 10.1016/j.ultrasmedbio.2020.06.018.

[66] S. K. Samijo *et al.*, "Wall shear stress in the human common carotid artery as function of age and gender," *Cardiovascular Research*, vol. 39, pp. 515-522, 1998.

[67] A. M. Moerman *et al.*, "The Correlation Between Wall Shear Stress and Plaque Composition in Advanced Human Carotid Atherosclerosis," *Front Bioeng Biotechnol*, vol. 9, p. 828577, 2021, doi: 10.3389/fbioe.2021.828577.

[68] R. El Sayed *et al.*, "Assessment of Complex Flow Patterns in Patients With Carotid Webs, Patients With Carotid Atherosclerosis, and Healthy Subjects Using 4D Flow MRI," *J Magn Reson Imaging*, vol. 59, no. 6, pp. 2001-2010, Jun 2024, doi: 10.1002/jmri.29013.

[69] S. W. Lee, L. Antiga, J. D. Spence, and D. A. Steinman, "Geometry of the carotid bifurcation predicts its exposure to disturbed flow," *Stroke*, vol. 39, no. 8, pp. 2341-7, Aug 2008, doi: 10.1161/STROKEAHA.107.510644.

[70] M. Markl *et al.*, "In vivo wall shear stress distribution in the carotid artery: effect of bifurcation geometry, internal carotid artery stenosis, and recanalization therapy," *Circ Cardiovasc Imaging*, vol. 3, no. 6, pp. 647-55, Nov 2010, doi: 10.1161/CIRCIMAGING.110.958504.

[71] A. M. Hoving, E. E. de Vries, J. Mikhal, G. J. de Borst, and C. H. Slump, "A Systematic Review for the Design of In Vitro Flow Studies of the Carotid Artery Bifurcation," *Cardiovasc Eng Technol*, vol. 11, no. 2, pp. 111-127, Apr 2020, doi: 10.1007/s13239-019-00448-9.

[72] J. M. K. De Bakker, C. L. De Korte, and A. Saris, "Cascaded Plane Wave Ultrasound for Blood Velocity Vector Imaging in the Carotid Artery," *IEEE Trans Ultrason Ferroelectr Freq Control*, vol. 71, no. 3, pp. 366-379, Mar 2024, doi: 10.1109/TUFFC.2024.3355712.

[73] L. T. Jorgensen, M. B. Stuart, and J. A. Jensen, "Transverse oscillation tensor velocity imaging using a row-column addressed array: Experimental validation," *Ultrasonics*, vol. 132, p. 106962, Jul 2023, doi: 10.1016/j.ultras.2023.106962.

[74] F. Varray, S. Salles, L. Petrusca, and H. Liebgot, "3D+t Vector Flow Imaging with Transverse Oscillations and Doppler Estimator," presented at the 2019 IEEE International Ultrasonics Symposium (IUS), 2019.

[75] J. Voorneveld *et al.*, "4-D Echo-Particle Image Velocimetry in a Left Ventricular Phantom," *Ultrasound Med Biol*, vol. 46, no. 3, pp. 805-817, Mar 2020, doi: 10.1016/j.ultrasmedbio.2019.11.020.